Acta Oceanol. Sin., 2019, Vol. 38, No. 4, P. 47–57
https://doi.org/10.1007/s13131-018-1224-2
http://www.hyxb.org.cn
E-mail: hyxbe@263.net

Seasonal variation of water transport through the Karimata Strait

Yan Wang[1, 2], Tengfei Xu[1, 2], Shujiang Li[1, 2], R. Dwi Susanto[3, 4], Teguh Agustiadi[5], Mukti Trenggono[6], Wei Tan[1, 2], Zexun Wei[1, 2*]

[1] Key Laboratory of Marine Science and Numerical Modeling, First Institute of Oceanography, Ministry of Natural Resources, Qingdao 266061, China

[2] Laboratory for Regional Oceanography and Numerical Modeling, Pilot National Laboratory for Marine Science and Technology (Qingdao), Qingdao 266237, China

[3] Department of Atmospheric and Oceanic Science, University of Maryland, College Park, Maryland 20742, USA

[4] Faculty of Earth Sciences and Technology, Bandung Institute of Technology, Bandung 40116, Indonesia

[5] Agency for Marine & Fisheries Research, Ministry of Marine Affairs and Fisheries, Jakarta 10110, Indonesia

[6] Faculty of Fisheries and Marine Science, Jenderal Soedirman University, Purwokerto 53123, Indonesia

Received 12 February 2018; accepted 18 May 2018

Abstract

Four trawl-resistant bottom mounts, with acoustic Doppler current profilers (ADCPs) embedded, were deployed in the Karimata Strait from November 2008 to June 2015 as part of the South China Sea-Indonesian Seas Transport/Exchange and Impact on Seasonal Fish Migration (SITE) Program, to estimate the volume and property transport between the South China Sea and Indonesian seas via the strait. The observed current data reveal that the volume transport through the Karimata Strait exhibits significant seasonal variation. The winter-averaged (from December to February) transport is –1.99 Sv (1 Sv=1×10^6 m^3/s), while in the boreal summer (from June to August), the average transport is 0.69 Sv. Moreover, the average transport from January 2009 to December 2014 is –0.74 Sv (the positive/negative value indicates northward/southward transport). May and September are the transition period. In May, the currents in the Karimata Strait turn northward, consistent with the local monsoon. In September, the southeasterly trade wind is still present over the strait, driving surface water northward, whereas the bottom flow reverses direction, possibly because of the pressure gradient across the strait from north to south.

Key words: Karimata Strait, water transport, seasonal variation, South China Sea throughflow

Citation: Wang Yan, Xu Tengfei, Li Shujiang, Susanto R. Dwi, Agustiadi Teguh, Trenggono Mukti, Tan Wei, Wei Zexun. 2019. Seasonal variation of water transport through the Karimata Strait. Acta Oceanologica Sinica, 38(4): 47–57, doi: 10.1007/s13131-018-1224-2

1 Introduction

The Karimata Strait (KS) and Gaspar Strait between Sumatra Island and Kalimantan Island are two important channels connecting the South China Sea (SCS) and the Indonesian seas. The KS is located between Belitung Island and Kalimantan Island with a width of 220 km and a depth of 18–50 m. The Gaspar Strait is located between Bangka Island and Belitung Island. Its width is approximately half that of the KS, and the depth is shallower than 30 m (Fig. 1a). For convenience, we collectively refer to these straits as the KS in the current study. The KS is important for the water transportation. In the boreal winter, Pacific water enters the SCS through the Luzon Strait and joins the Indonesian seas through the southern exits of the SCS, such as the KS, Mindoro Strait and Balabac Strait (Qu et al., 2005). Therefore, this flow is a branch of the Indonesian throughflow (ITF), also known as the South China Sea throughflow (SCSTF) (Fang et al., 2002, 2005; Qu et al., 2005). The annual average contribution of the KS transport to the transport of the ITF is approximately 13% (He et al., 2015). As one of the outflow passages of the SCSTF, the KS conveys the warm and fresh SCS surface water into the Java Sea, playing an important role not only on the heat and freshwater transport of the ITF, but also in maintaining the salt and heat balance of the SCS (Qu et al., 2006).

The earliest research on water exchange between the SCS and the Indonesian seas through the KS was based on ship drift data (Wyrtki, 1961), with an estimated volume transport of –4.5 Sv (1 Sv=1×10^6 m^3/s) in the boreal winter, and 3 Sv in the boreal summer (positive/negative value indicates northward/south-

Foundation item: The National Key Research and Development Program of China under contract No. 2016YFC1402604; the Scientific and Technological Innovation Project financially supported by Qingdao National Laboratory for Marine Science and Technology under contract No. 2015ASKJ01; the SOA Program on Global Change and Air-Sea Interactions under contract Nos GASI-IPOVAI-03, GASI-IPOVAI-02 and GASI-IPOVAI-01-02; the National Natural Science Foundation of China under contract Nos 40476025, 41876027 and 41506036; the China-Indonesia Maritime Cooperation Fund under contract No. U1406405; the National Science Foundation of the United States under contract No. OCE-07-25935; the Office of Naval Research of United States under contract No. N00014-08-01-0618.

*Corresponding author, E-mail: weizx@fio.org.cn

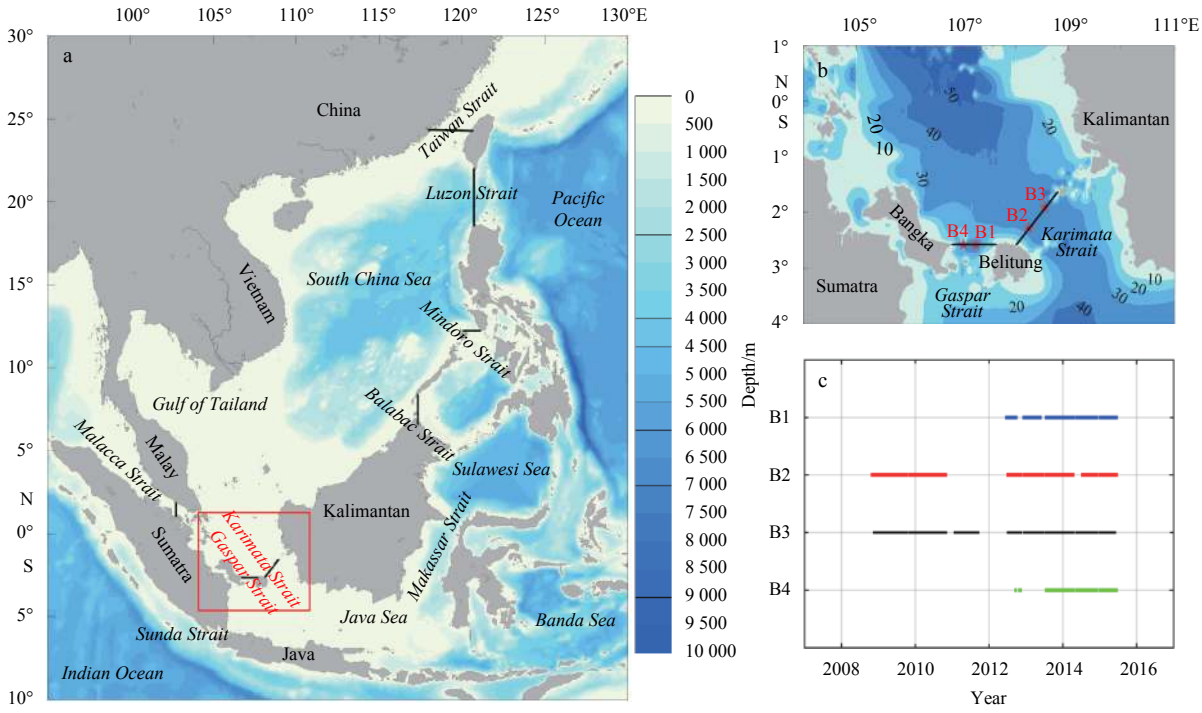

Fig. 1. Geography of the SCS and Indonesian seas (a); solid lines indicate the transections for the calculation of interocean transports; geography of the KS (contour depth unit: m) and location of the trawl-resistant bottom mount sites (b); solid lines indicate the Gaspar section and the Karimata section respectively; and time length of the valid ADCP data (c).

ward transport). In the subsequent decades, the KS transport has mainly been studied using numerical simulations, producing annual mean volume transport values with wide variation, ranging from –0.3 to –4.4 Sv (Lebedev and Yaremchuk, 2000; Fang et al., 2003, 2005, 2009; Yaremchuk et al., 2009; Du and Qu, 2010; Liu et al., 2011; Wei et al., 2016). Although the simulation results markedly differ in the terms of the quantity of transport, there is a general consensus that the KS transport is northward in summer, and southward and stronger in winter, while the annual average net transport is from the SCS into the Java Sea.

Water exchange through the KS is mainly driven by monsoon (Fang et al., 2010). When the northwesterly (southeasterly) monsoon prevails in the boreal winter (summer), the water flows southward (northward). In addition, there is a north-south sea surface slope in the KS in the boreal winter, suggesting that the pressure gradient along the strait is also one of the driving contributors of the SCSTF (Fang et al., 2010). On an interannual timescale, the SCSTF is affected by the El Niño-Southern Oscillation (ENSO), with increased transport through the Luzon Strait, the KS and the Mindoro Strait during El Niño (Wang et al., 2006; Tozuka et al., 2009; He et al., 2015), which further modulates the interannual variability of the ITF (Liu et al., 2007). In addition to the ENSO, the KS transport is affected by the Indian Ocean dipole (IOD). One previous study reported that more water enters the Indian Ocean from the SCS through the KS in the positive IOD phase (He et al., 2015). Preliminary modeling experiments found that the buoyant freshwater from the SCS forces the ITF into a deeper level (near the thermocline) and reduces its heat transport in the Makassar Strait (Gordon et al., 2003; Tozuka et al., 2007).

To date, only two studies (Fang et al., 2010; Susanto et al., 2013) have estimated the KS transport based on direct ocean current observations. The earlier of the two studies reported that the volume, heat and fresh water transports through the KS in the boreal winter of 2007–2008 were –3.6 Sv, –0.36 PW (1 PW = 1×10^{15} W) and –0.14 Sv, respectively. The later estimation by Susanto et al. (2013) using observational data from December 2007 to October 2008, indicated that the average volume, heat and freshwater transports from December 2007 to March 2008 (winter) were –2.7 Sv, –0.30 PW, –0.18 Sv, respectively; those from May to September 2008 (summer) were 1.2 Sv, 0.14 PW, 0.12 Sv, respectively; and those for the entire record were –0.5 Sv, –0.05 PW, –0.01 Sv, respectively. The data used in both of these previous studies were based on observations conducted by the South China Sea-Indonesian Seas Transport/Exchange and Impact on Seasonal Fish Migration (SITE) Program, which was established jointly by scientists from China, Indonesia, and the United States in October 2006. In the current paper, to provide a more accurate estimation, we investigate the transport through the KS based on observational data from the SITE program during the period from November 2008 to June 2015. First, we introduce the data set and methods used in data processing, and then describe the seasonal variation of volume transport via the KS. Finally, we discuss the causes of its seasonal variation and the importance of the KS transport in maintaining heat and freshwater balance in the SCS.

2 Data and methods

2.1 *Data*

The SITE project has been in operation since October 2006. By July 2015, 18 cruises have been carried out and four Trawl-Resistant Bottom Mount (TRBM) stations have been deployed in the KS. Each of the stations is equipped with a 300-kHz acoustic Doppler current profiler (ADCP), observing upwards from the seafloor with a layer depth of 2 m and a sampling time interval of 20 or 60 min. These ADCP parameters have a measurement

range of 165 m, covering the full depth of the observation station. The positions of these stations are: B1 (2°34.625′ S, 107°15.033′ E), B2 (2°16.689′ S, 108°14.816′ E), B3 (1°54.618′ S, 108°32.703′ E) and B4 (2°34.623′ S, 107°0.899′ E), in which B1 and B4 are on the Gaspar section, while B2 and B3 are on the Karimata section (Fig. 1b). The ADCP data obtained from Stas B2 and B3 cover the period from 7 November 2008 to 12 June 2015, while those from Stas B1 and B4 cover from 23 June 2012 to 10 June 2015. There are some gaps in the data due to equipment problems. To fill these gaps, we use a regression method following Fang et al. (2010) to reconstruct the current data time series, which will be introduced in detail below. For processing current data, we use the Version 2.0 of the Cross Calibrated Multi-Platform (CCMP v2.0) daily wind data obtained from http://www.remss.com/measurements/ccmp (Atlas et al., 2011), and the daily absolute dynamic topography (ADT) data obtained from http://www.aviso.altimetry.fr/duacs/. Both data have a horizontal resolution of 0.25°×0.25°. The bathymetry adopted for the volume estimation is ETOPO1, obtained from http://www.ngdc.noaa.gov/mgg/global/, which has a high horizontal resolution of 1′ ×1′.

In addition to the above-mentioned data, we also use the GLBa0.08 dataset, a product of the Hybrid Coordinate Ocean Model (HYCOM). The hybrid coordinate is isopycnal in the open, stratified ocean, but smoothly reverts to a terrain-following coordinate in shallow coastal regions, and to z-level coordinates in the mixed layer and unstratified regions (Bleck and Douglas, 1981). It maintains the significant advantages of an isopycnal model in stratified regions, and allows finer vertical resolution near the surface and in shallow coastal areas, providing a better representation of the upper ocean physics (Metzger et al., 2010). HYCOM assimilates available satellite altimeter observations and *in-situ* sea surface temperature as well as available *in-situ* vertical temperature and salinity profiles from XBTs, ARGO floats and moored buoys (Cummings, 2005). The horizontal resolution of this product has an average spacing of approximately 7 km spacing on average. There are 32 vertical layers and the bathymetry is derived from a quality controlled NRL DBDB2 dataset. The velocity profile of the product in the Luzon Strait is very close to that observed (Zhang et al., 2010) and it has advantages in simulating the deep circulation in the SCS (Xie et al., 2013). We use daily average velocity, temperature, salinity and surface flux data of this product from January 2009 to December 2014.

2.2 *Data processing method*

After applying quality control to each time series data set for the four stations, we calculate the daily mean currents and interpolate them into standard layers with a vertical resolution of 2 m. Given the problems caused by surface reflection contamination of the ADCP data, we replace the data of surface layer data with linearly extrapolated data from the second and third layers according to the constant shear assumption (Sprintall et al., 2009; Fang et al., 2010).

Surface wind plays a dominant role in the KS, given its shallow depth. In addition, there is also a downstream sea surface slope across the strait in the boreal winter that affects the flow through the strait as reported by Fang et al. (2010). To reconstruct the time series of the current of each station, we establish a regression model between the current speed and the two factors, as mentioned above. Since this study focuses on transport through the KS, it is the current component perpendicular to the Gaspar section and Karimata section that matters for calculating transport. The Gaspar Strait is a north-south strait, and the direction along the strait axis is 0° (referenced to true north). Regarding the KS, the downstream direction along the strait axis is 309°. The current vectors are decomposed into along-strait component, u, and a cross-strait component, v, which can be calculated from

$$\begin{cases} u = w\cos(\theta - \psi), \\ v = -w\sin(\theta - \psi), \end{cases} \tag{1}$$

where w and θ are the speed and direction of the current, and ψ is the downstream direction of the Gaspar section or the Karimata section, equaling 0° and 309°, respectively. In this study, "velocity" of the Gaspar section and the Karimata section refer to the along-strait velocity (ASV), with negative values indicating flow into the Java Sea.

We analyzed the simultaneous correlation between the ASV of each station and the ADT of nearby waters. Since the distributions of correlation coefficients at all stations are similar, only the results from Sta. B3 are shown in Fig. 2 as an example. Downstream ADT is clearly negatively correlated with the ASV of Sta. B3, whereas the correlation is positive upstream. We select Areas A and B in the up and downstream region respectively, where the correlation is most significant. The difference between the regional averaged ADT of Area A (4.375–5.625°S, 106.125–108.625°E) and Area B (0.625°S–0.625°N, 106.125–108.625°E) is used to represent the influence of the sea surface slope induced pressure gradient on the ASV of Sta. B3 and is referred to as ΔADT hereinafter.

Assuming that the variation of the ASV is mainly caused by variation of local wind and sea surface slope, the ASV can be linearly estimated as

$$\mathrm{ASV} = u_0 + a_1 \times U + a_2 \times V + a_3 \times \Delta\mathrm{ADT} + \varepsilon, \tag{2}$$

where U and V are the zonal and meridional component of local wind, u_0 is the intercept value, representing basic flow without local wind and pressure gradient, a_1, a_2 and $a_3$are the regression

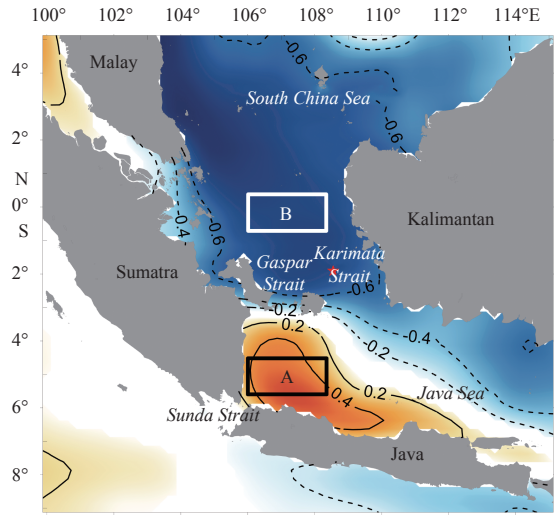

Fig. 2. Correlation coefficients between vertical mean along strait velocity of B3 and ADT during the observation period. The red star denotes the location of Sta. B3. Rectangles A and B represent areas where the ADT is selected for the estimation of pressure gradient across the strait. Correlation coefficients of the shaded area exceed the 95% confidence level.

coefficients, and ε is the residual. The multiple linear regression analysis is used for all of the observed ASV of Sta. B3 at each layer, and the corresponding regression coefficients are shown in Table 1. Without the influence of the local wind and pressure gradient, u_0 has a maximum value of –22.5 cm/s at the sea surface and gradually decreases with depth. This result differs from a previous study by Fang et al. (2010), in which u_0 was almost independent of depth. In addition, the correlation coefficients between the observed and regression-derived ASV in Fang et al.' s (2010) study decrease with depth, whereas, in the current study, the correlation coefficients increase with depth. It shows that the regression result is improved when the pressure gradient across the strait is taken into consideration. Moreover, the correlation coefficients are generally high (>0.8), suggesting the possibility that the regression-derived ASV can be used to fill the gaps where the observations are not available.

Table 1. Regression coefficients of ASV on local wind and pressure gradient at Sta. B3

Depth/m	u_0/cm·s^{-1}	a_1	a_2	a_3	r
0.00	–22.52	–2.10	1.52	98.52	0.82
2.00	–20.39	–2.13	1.92	112.51	0.84
4.00	–18.95	–2.13	1.79	115.63	0.85
6.00	–18.61	–2.04	1.65	113.02	0.86
8.00	–18.43	–1.79	1.56	118.38	0.86
10.00	–17.00	–1.67	1.44	120.96	0.87
12.00	–16.68	–1.50	1.41	119.80	0.88
14.00	–16.40	–1.35	1.38	118.34	0.88
16.00	–16.06	–1.20	1.36	116.17	0.88
18.00	–15.73	–1.04	1.36	113.18	0.89
20.00	–15.40	–0.91	1.36	110.37	0.89
22.00	–15.06	–0.79	1.35	107.24	0.90
24.00	–14.69	–0.70	1.35	103.49	0.90
26.00	–14.27	–0.63	1.36	99.21	0.91
28.00	–13.82	–0.58	1.38	94.31	0.91
30.00	–13.39	–0.56	1.40	88.84	0.92
32.00	–12.83	–0.54	1.35	84.16	0.91
34.00	–12.37	–0.51	1.35	79.29	0.91
36.00	–11.87	–0.49	1.34	74.59	0.91
38.00	–11.30	–0.47	1.30	69.86	0.91
40.00	–10.53	–0.45	1.24	64.18	0.91

Note: r is the correlation coefficient between the observed and regression-derived ASV.

After the reconstruction of the ASV, the daily values of ASV on a section can be estimated by interpolating or extrapolating the daily values at each station layer by layer along terrain-following surfaces. The bathymetry used here is from ETOPO1. We adopt the logarithmic-profile-cubic-spline interpolation method, which is described in detail in Appendix A of Fang et al. (2010).

The volume transport through a section A can be calculated using the following formula:

$$F_{\mathrm{v}} = \int_A u \mathrm{d}A, \tag{3}$$

where dA denotes a cell area of Section A, and u is the ASV of the corresponding cell obtained with the method mentioned above.

Following Fang et al. (2010) and Susanto et al. (2013), the heat transport through Section A can be calculated from

$$F_{\mathrm{h}} = \rho C_{\mathrm{P}} \int_A (T - T_0)\, u \mathrm{d}A, \tag{4}$$

where ρ is the density of sea water, and can be taken as 1 021 kg/m^3 for a mean temperature of 28°C and a mean salinity of 33; C_{p} is the specific heat capacity; T is the water temperature; and T_0=3.72°C is a reference temperature (Schiller et al., 1998; Fang et al., 2010). ρC_{P} can be regarded as the heat capacity per unit volume, and 4 100 J/(kg·K) is taken for the above temperature and salinity, following Fang et al. (2010).

The salt and freshwater transport can be calculated from

$$F_{\mathrm{s}} = \rho \int_A S u \mathrm{d}A, \tag{5}$$

$$F_{\mathrm{w}} = \rho \int_A \left[(S_0 - S) / S_0 \right] u \mathrm{d}A, \tag{6}$$

where S is the salinity and S_0 is the reference salinity taken as 34.62 following Fang et al. (2010).

3 Results and discussion

3.1 *Volume transport*

Figure 3 shows the time average ASV of the Gaspar section and Karimata section from the observational data of the SITE program, respectively. According to the bathymetry of ETOPO1, the Gaspar section is approximately 90 km wide, with a maximum depth of 34 m. The average surface velocity is –25 cm/s and the average bottom velocity is approximately –9 cm/s. The major axis of the current is located in the middle of the strait. The Karimata section has a width of 120 km and a maximum depth of 40 m. The surface velocity is approximately –22 cm/s. The bottom flow velocity is approximately –9 cm/s. The major current axis is also located in the middle of the strait. Although the velocity of the surface layer in the Gaspar section is relatively high, the –15 cm/s velocity contour is only confined to a shallow depth of 8 m, while in the Karimata section, the contour of –15 cm/s velocity reaches up to 20 m.

Figure 4 demonstrates the vertical distribution of monthly volume transport through the Gaspar section and Karimata section calculated from the observational data and HYCOM assimilation data respectively. The southward (from the SCS to the Java Sea) transport begins in mid-September and terminates in early May, while the northward (from the Java Sea to the SCS) transport begins in mid-May and terminates in early September (Figs 4a, b). Susanto et al. (2013) reported the existence of a weak southward bottomflow in the boreal summer of 2008 using data from Sta. A2, which was deployed during the first stage of the SITE program and is located approximately 100 km northwest of Sta. B3. While in the mean state, northward flow dominates from March to August, and the reversal southward bottomflow only occurs in September at Sta. B3. Transport distribution in the HYCOM data shows a similar seasonal reversal transport to that in the observational data in the current study, and both the amplitude and structure are similar (Figs 4c, d). The transition time in the HYCOM data lags behind that in the observational data by approximately half a month in September (Figs 4c, d), suggesting that the HYCOM data are not sufficiently accurate in simulating the transition of the transport through the KS. In addition, the volume transport through the Gaspar Strait in HYCOM is weaker

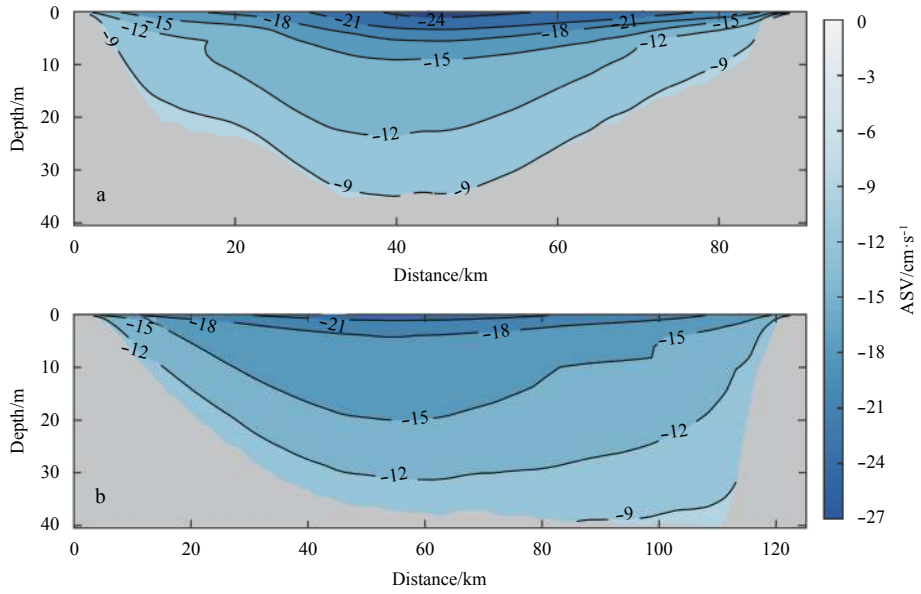

Fig. 3. Mean ASV of the Gaspar section (a) and the Karimata section (b) from SITE data. The contour interval is 3 cm/s.

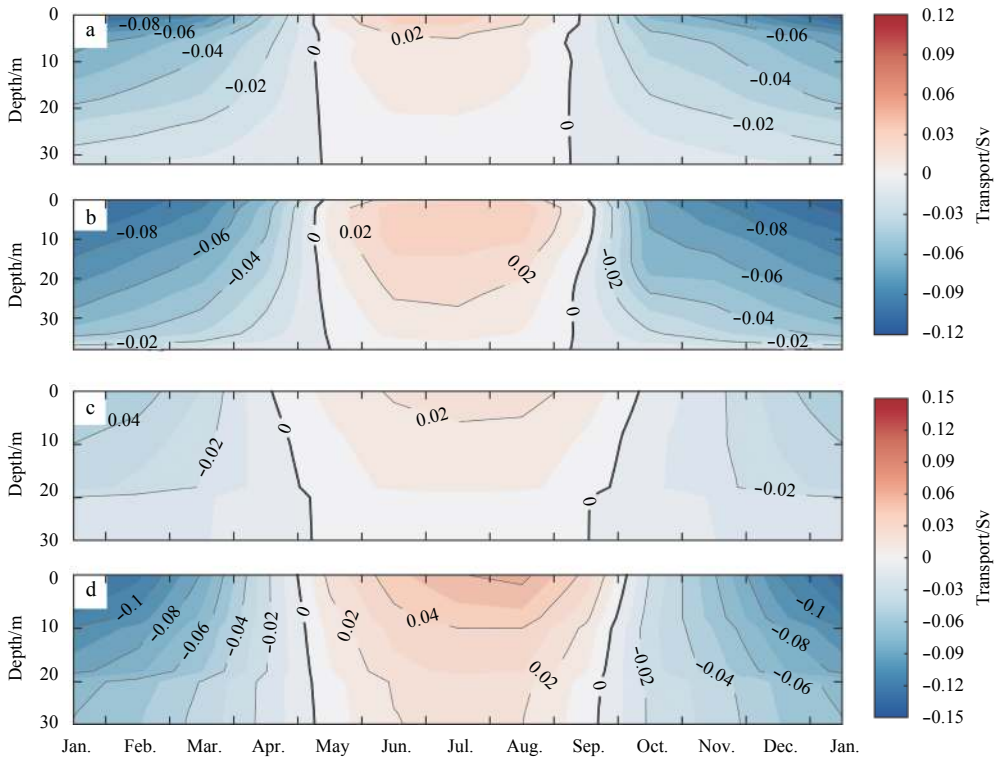

Fig. 4. Monthly climatology of volume transport of Gaspar section (a) and Karimata section (b) from SITE data, and Gaspar section (c) and Karimata section (d) from HYCOM data. Positive/negative value indicates northward/southward transport, black lines are 0 contour lines. Vertical resolution of HYCOM data has been improved from 10 m into 2 m by linear interpolation, the same resolution as observations, for comparison.

than that in the observational data.

Full depth transport of each section is shown in Fig. 5. It can be seen that the maximum southward transport occurs in January and the maximum northward transport occurs in July for both sections. In the boreal winter (from December to February), the average transport of the Gaspar section is –0.71 Sv, while average transport of the Karimata section is –1.28 Sv, and the sum of these two sections is –1.99 Sv. In the boreal summer (from June to August), the average transport of the Gaspar section is 0.22 Sv, while the average transport of the Karimata section is 0.46 Sv, and the sum is 0.69 Sv. The record from January 2009 to December 2014 is –0.74 Sv, which is larger than Susanto et al. (2013). Volume transport from the HYCOM data is very close to that in the observational data, except for a late transition time in

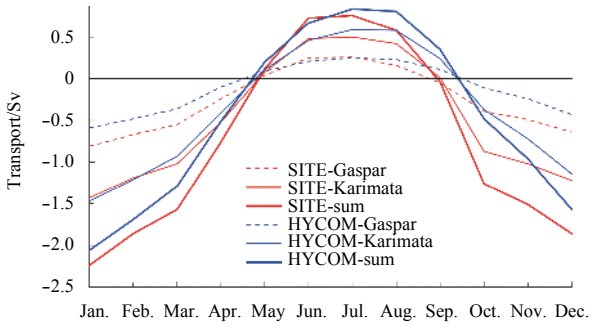

Fig. 5. Monthly climatological volume transport of the Gaspar section and Karimata section. Positive/negative value indicates northward/southward transport. Red lines demonstrate results of observations, and blue lines demonstrate that of HYCOM data. Thick lines demonstrate the sum of transport through the Gaspar section and Karimata section.

September (Fig. 5). Therefore, the HYCOM assimilation data appear to effectively demonstrate the seasonal variation of the heat and freshwater transport in the KS.

3.2 *Influence of sea surface wind & sea surface slope on volume transport*

The circulation in the SCS is mainly controlled by the East Asian monsoon and the interactions with adjacent regions (Su, 2005). As an outflow strait of the SCSTF, the KS is also under the influence of the monsoon and water exchange. Thus, we mainly discuss the two factors in terms of the dynamics of the seasonal variations of the KS transport.

The seasonal characteristics of the SCS circulation indicate that the monsoon is the main driving force (Wyrtki, 1961). In winter (from December to February), the prevailing northeasterly monsoon occupies the entire SCS (Figs 6a, b, l) and the maximum wind speed is approximately 10 m/s. The northwestward Ekman transport induced by northeasterly monsoon strengthens the Kuroshio intrusion into the SCS (Wu and Hsin, 2012). The surface water is transported westward, and piles in the western boundary, forming a high sea surface height. A stable westward flow forms at approximately 20°N. In the south of Hainan Island, it turns southward and joins the western boundary current of the SCS along the continental shelf of the Indo-China Peninsula (Figs 7a, b, l). In the southern SCS, the northeasterly monsoon bifurcates into two branches: one turns westward at approximately 8°N which maintains the high sea level in the Gulf of Thailand, whereas, the other crosses the equator along the KS and turns into the northwesterly monsoon affected by the Coriolis force in the southern hemisphere. The western boundary current flows southward along the Malay Peninsula, and then enters the Java Sea through the KS and Gaspar Strait, forming the basin-scale SCSTF (Figs 7a, b, l). In the Java Sea, Ekman transport is driven by the northwesterly monsoon results in a water pileup in the northern Java Sea and southern Makassar Strait, while low sea level occurs near the Sunda Strait, east of Sumatra. In January, the northwesterly monsoon over the KS is the strongest in winter. Meanwhile, the pressure gradient formed by the southward sea surface slope across the strait favors the SCS water entering the Java Sea as well, causing the volume transport through the KS to reach the maximum level (Fig. 8).

The boreal spring (from March to May) is a monsoon transition period. From March to April, with the declining of the northeasterly monsoon, the high ADT in the Gulf of Thailand and the northern KS decreases, which further leads to the weakening of the KS transport. The southwesterly summer monsoon bursts in May and the basin scale cyclonic circulation disappears. Meanwhile low ADT appears in the Gulf of Thailand. Both the wind over the KS and the sea surface slope turns north, resulting in the reversal of transport through the KS (Fig. 8).

In the boreal summer (from June to August), most of the SCS basin is occupied by southwesterly monsoon, leading to the eastward transport of surface water. As a result, low ADT appears in the entire western boundary of the SCS. From June to July, driven by southwesterly monsoon, surface water from the Java Sea enters the SCS through the KS and flows northward along the coast of Malay Peninsula at a relatively low speed, and eventually joins in the northeastward Vietnam Coast Current (Figs 7f, g, h). This flow exists throughout the whole summer and contributes to the anti-cyclonic circulation in the southern SCS. In August, the along-strait components of southeasterly trade winds over the Karimata section are strongest, while the maximum northward sea surface slope appears in June (Fig. 8). The northward volume transport through the KS reaches its maximum level in July, which may be the result of the combined effects of the wind and sea surface slope.

In September, the onset of the northeasterly monsoon takes place in the northern SCS. Meanwhile the southern SCS is still occupied by the relatively weak southwesterly monsoon. As a result, a cyclonic circulation forms in the northern SCS when the anti-cyclonic circulation sustains in the southern SCS (Fig. 7i). In the KS, the sea surface water flows northward, consistent with the sea surface wind. However, the bottomflow has turned south by this time, the same direction as the pressure gradient (Fig. 8). This suggests that the southward pressure gradient across the strait causes the reversal of the bottom flow. From October to November, the northeasterly monsoon extends southward to the equator, and the anti-cyclonic circulation in the southern SCS disappears. Over the Gulf of Thailand and Sunda shelf north of the KS, the sea level increases. At this time, the southeasterly trade winds decay to 10°S and there is almost no wind over the KS. The pressure gradient caused by the north-south sea surface slope plays a major role in maintaining the southward KS transport (Fig. 8). From November to December, the SCSTF strengthens and directly invades into the Java Sea (Figs 7k, l), resulting in the significant increase of the KS volume transport. We speculate that both the monsoon and the sea surface slope are important factors influencing the seasonal variation of the KS volume transport. Local winds are the dominant force influencing the currents in the KS (Fang et al., 2010), and can change the sea surface height. However sea surface height variability is influenced by local wind stress as well as other factors, such as atmospheric pressure at sea level (Sterlini et al., 2016) and advection of ocean circulation. Regarding the KS, Ekman transport induced by wind stress and Sverdrup transport induced by basin-scaled wind stress curl in the SCS may affect the sea surface height near the KS, and further affect sea surface slope in the KS.

3.3 *Heat and freshwater transport*

On the basin average, the SCS receives heat of 0.1–0.2 PW from the atmosphere (Qu et al., 2009). Preliminary examination of the NCEP reanalysis data indicates that the precipitation in the SCS exceeds evaporation (P–E) by about 0.1 Sv, leading to the freshest sea surface in the region (Qu et al., 2009). On the long-term average this net heat and freshwater gain can only be bal-

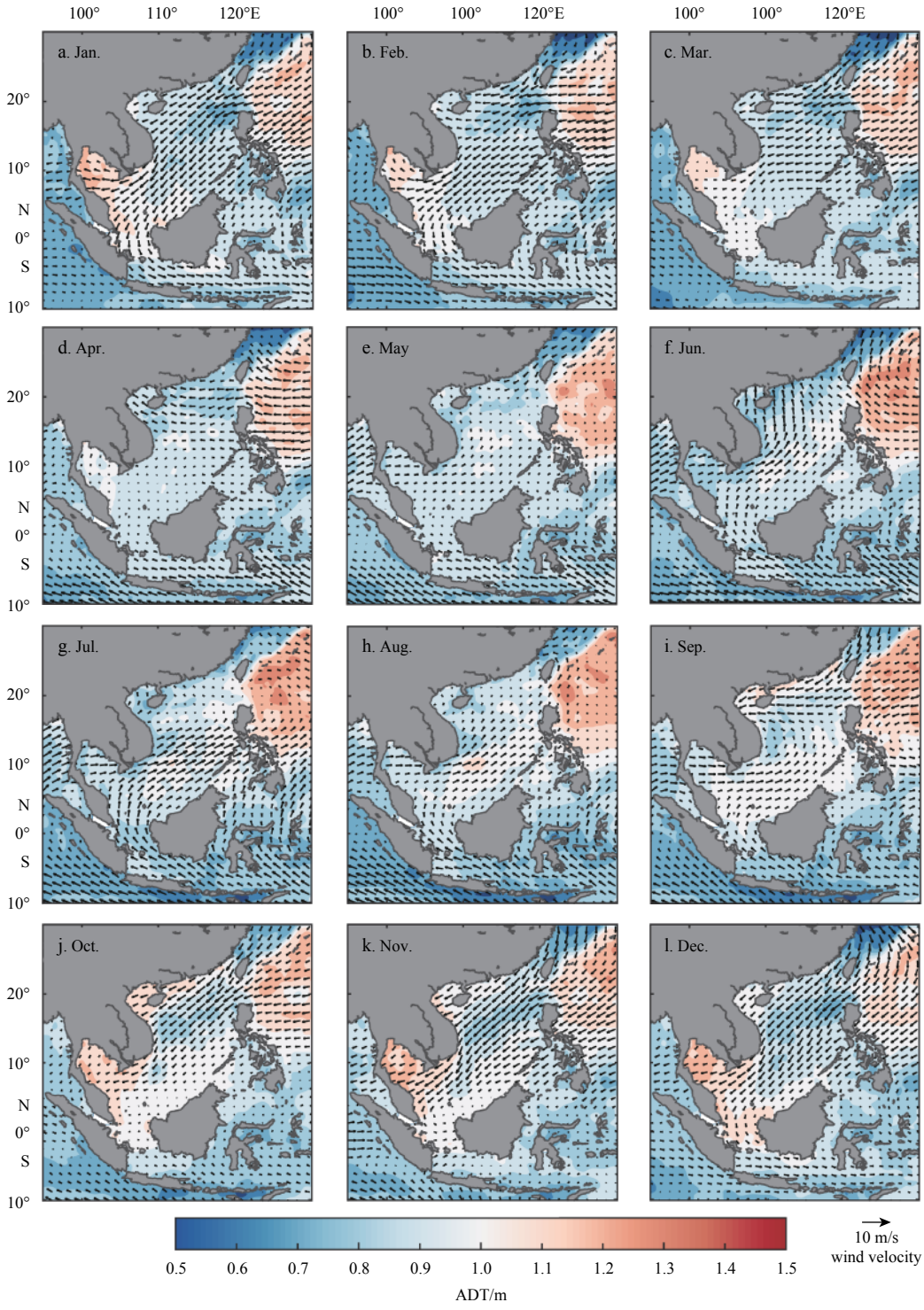

Fig. 6. Monthly climatology of sea surface wind velocity (vector, m/s) and ADT (contour, m) of the SCS. CCMP v2.0 wind data and AVISO altimeter data are used and averaged from 2008 to 2015.

anced by horizontal advection, with inflow of cold and salty water through the Luzon Strait and outflow of warm and fresh water through the Mindoro Strait and Karimata Strait (Qu et al., 2006). However, it is currently unclear how much heat and freshwater the KS transports, and whether these factors are crucial to SCS water exchange. To assess the importance of KS transport, we calculate heat and freshwater transport using HYCOM outputs. The selected sections for transport estimation are shown in Fig. 1a. For convenience, we refer to the sum of the transport through the Gaspar and Karimata section as the KS transport.

The average volume transport through the Balabac Strait and the Malacca Strait add up to –0.12 Sv, accounting for less than 3% of the inflow from the Luzon Strait, and the seasonal changes in these straits are so weak that they can be neglected. Figure 9 shows the monthly transport through the main channels around the SCS.

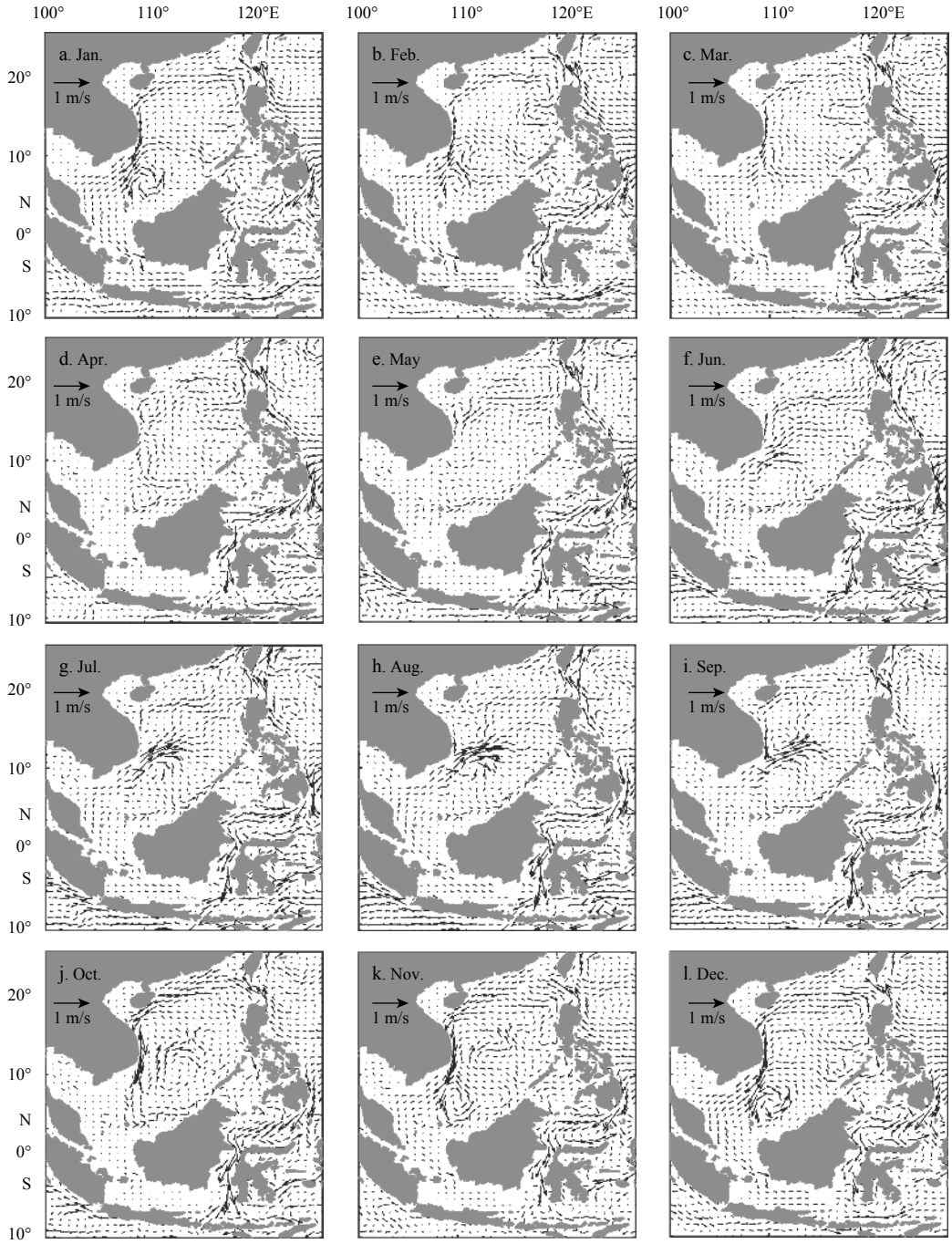

Fig. 7. Monthly climatology of sea surface velocity field of the upper 30 m in the SCS. HYCOM data are used and averaged from 2008 to 2015.

The Luzon Strait has a large inflow in winter, while the outflow through the Taiwan Strait is relatively small. The seawater exits the SCS mainly through the Mindoro Strait and the KS. In summer, the inflow from Luzon Strait weakens, and the surface water of the Java Sea enters the SCS through the KS. The seawater exits the SCS mainly through the Taiwan Strait and the Mindoro Strait (Fig. 10a). The variation of salt transport is similar to volume transport in all straits (Fig. 10b). In the mean state, seawater enters the SCS from the Luzon Strait and exits through the other straits. Annual mean volume transport and salt transport through the KS account for 10.6% and 9.9% of the volume and salt entering the SCS, respectively (Figs 9a, b).

Using HYCOM assimilation data, the SCS has a net heat gain (NHG) of 0.169 PW from the atmosphere, and 0.261 PW entering through the Luzon Strait. The heat flows out through the KS is 0.051 PW, accounting for 11.6% of total heat gain of the SCS (Fig. 9c).

The annual average freshwater flux from atmosphere into the SCS is 0.113 Sv, and the freshwater exits through all straits of the SCS. Annual average freshwater transport through the KS is 0.030 Sv, which is the largest among all the straits in the SCS, accounting for approximately 26.3% of the total freshwater entering the SCS (Fig. 9d). The maximum southward freshwater transport through the KS is 0.18 Sv, in January, but in summer the freshwater trans-

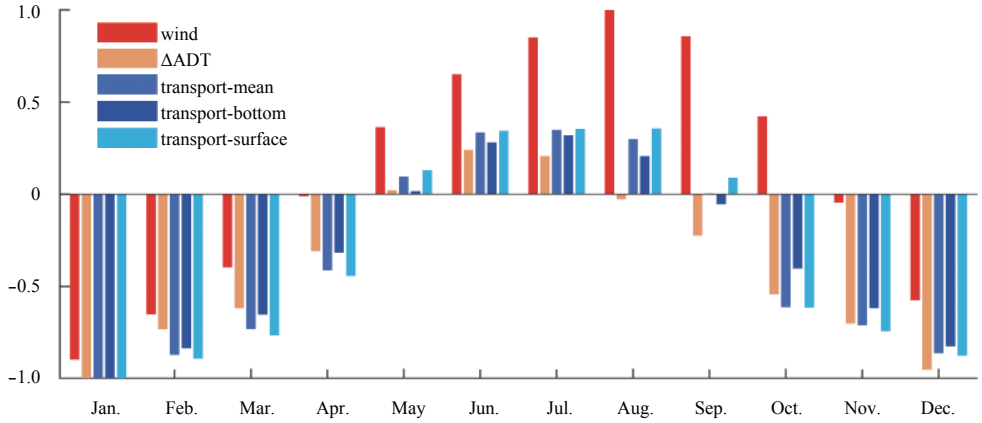

Fig. 8. Monthly climatology of the along-strait component of wind, ΔADT and volume transport through the Karimata section normalized by their maximun. Positive/negative value indicates northward/southward.

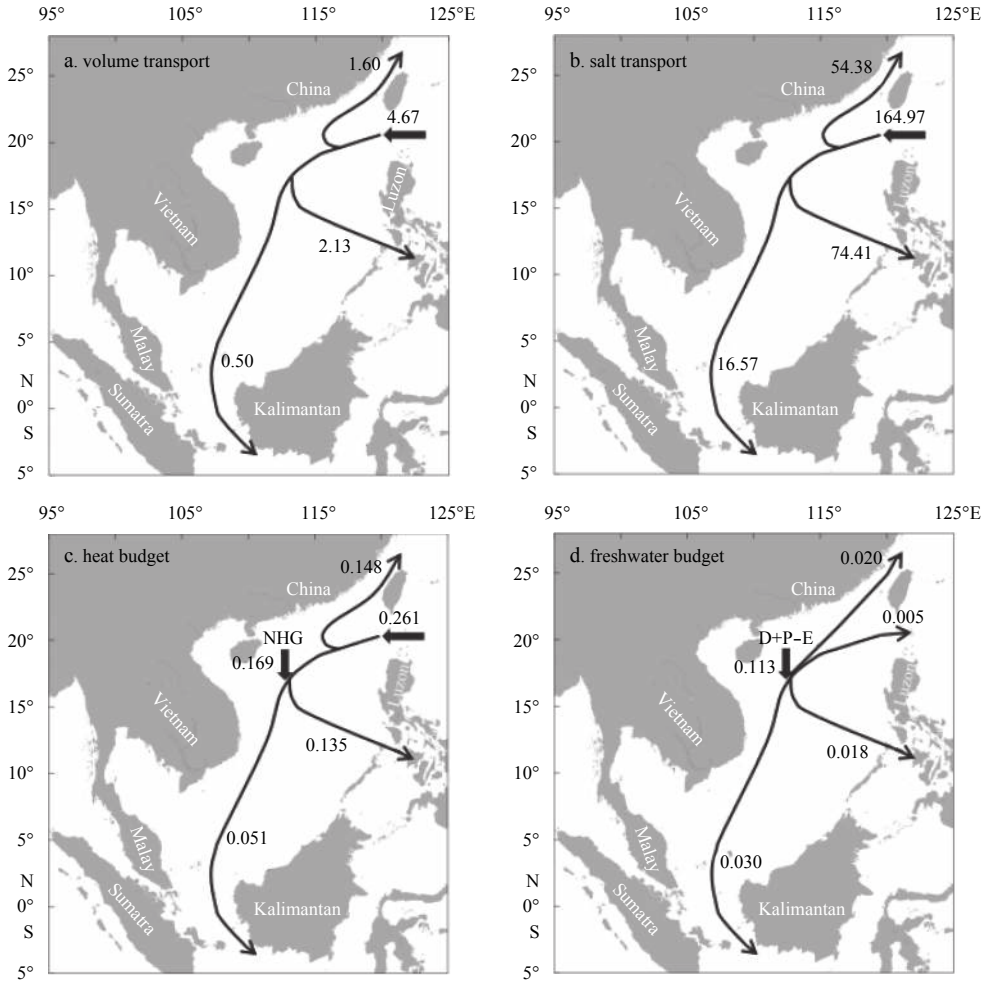

Fig. 9. Annual mean volume transport (Sv) (a), salt transport (Gg/s) (b), heat budget (PW) (c), and freshwater budget (Sv) (d) through the main straits in the SCS from 2008 to 2015 in HYCOM data. NHG refers to net heat gain and D+P–E refers to discharge of rivers plus precipitation minus evaporation.

port turns northward and the maximum is 0.08 Sv in July. The seasonal amplitude reaches 0.26 Sv (Fig. 10d). This result is consistent with the findings of Susanto et al. (2013). It shows that the freshwater transport through the KS has an important influence on the SCS freshwater balance.

4 Summary

The SCSTF has an important influence on the heat capacity of the SCS and the vertical structure and path of the ITF (Qu et al., 2009), and the KS is an important exit for the SCSTF. In the current study, the seasonal variation of the water transport in the KS

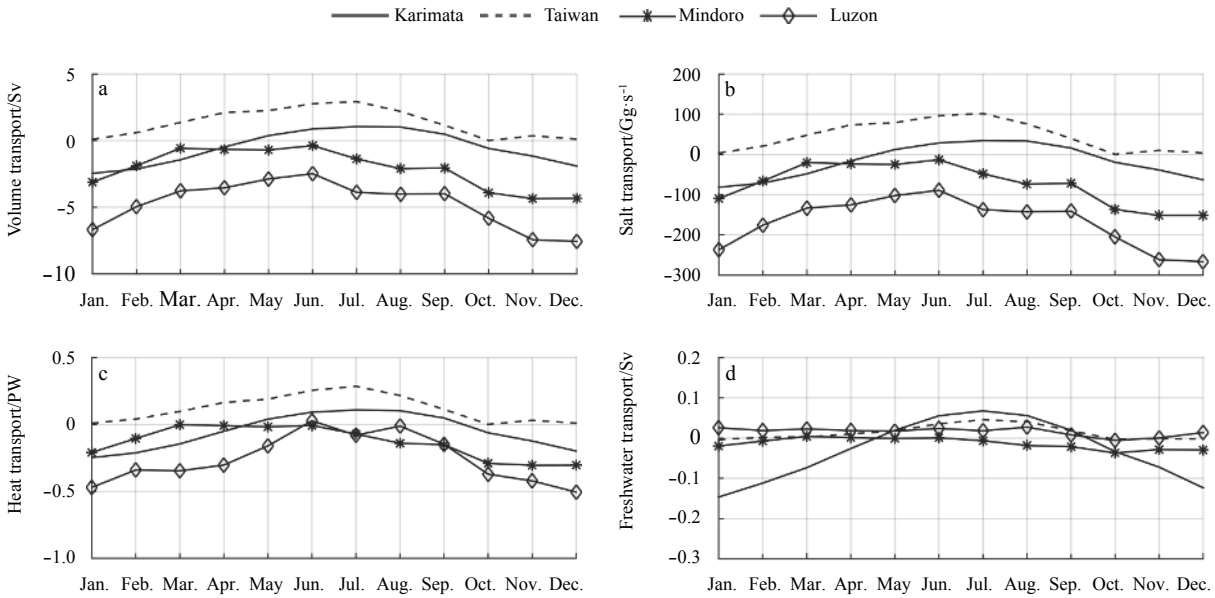

Fig. 10. Monthly climatology of volume (a), salt (b), heat (c) and freshwater transport (d) through main passages of the SCS from HYCOM data.

is investigated using the ADCP observational data from the SITE program from November 2008 to June 2015. In the boreal winter (from December to February), the average transport of the KS is –1.99 Sv. In the boreal summer (from June to August), the average transport is 0.69 Sv. The average during the record from January 2009 to December 2014 is –0.74 Sv, which is greater than the estimate made by Susanto et al. (2013), and is near the small end of previous numerical model estimates varying from –0.3 to –4.4 Sv (Lebedev and Yaremchuk, 2000; Fang et al., 2003, 2005, 2009; Yaremchuk et al., 2009; Du and Qu, 2010; Liu et al., 2011; Wei et al., 2016). Of these, Wei et al. (2016) provide the closest estimate of –0.7 Sv. Seasonal changes of the currents in the KS are dominated by monsoon, while the pressure gradient caused by sea surface slope across the Strait is an important factor as well. May and September are the transition period of the current in the KS. In September, southeasterly trade winds still occupy the sea surface of the strait, driving surface water northward, but the bottom flow has reversed its direction, possibly due to the southward pressure gradient across the strait. The heat and freshwater transport estimated using HYCOM assimilation data are 0.051 PW and 0.030 Sv, accounting for 11.6 % and 26.3% of the total flux entering the SCS, respectively, indicating that the KS is an important freshwater exit of the SCS.

It should be noted that the HYCOM uses vertical mixing coordinates, resulting in the problem of nonconservation of flux when the outputs are interpolated to gridded products, but the magnitude and variation can still be used as a reference for transport estimation.

Previous studies have revealed that SCSTF through the KS contains a strong ENSO signal and appears to have a notable impact on the ITF. Therefore, the KS may also be an important pathway for conveying the Pacific influence to the Indian Ocean (Qu et al., 2005, 2006). In addition, the heat advection of SCSTF through the KS and ITF, makes significant contributions to the interannual variability of the equatorial eastern Indian Ocean (EIO) upwelling (Chen et al., 2016). The impact of the KS transport on the environment of the SCS and Java Sea, and its role in the Indo-Pacific climate warrant further research.

References

Atlas R, Hoffman R N, Ardizzone J, et al. 2011. A cross-calibrated, multiplatform ocean surface wind velocity product for meteorological and oceanographic applications. Bulletin of the American Meteorological Society, 92(2): 157–174, doi: 10.1175/2010BAMS2946.1

Bleck R, Douglas B. 1981. Initial testing of a numerical ocean circulation model using a hybrid (quasi-isopycnic) vertical coordinate. Journal of Physical Oceanography, 11(6): 755–770, doi: 10.1175/1520-0485(1981)011<0755:ITOANO>2.0.CO;2

Chen Gengxin, Han Weiqing, Li Yuanlong, et al. 2016. Interannual variability of equatorial eastern Indian Ocean upwelling: Local versus remote forcing. Journal of Physical Oceanography, 46(3): 789–807, doi: 10.1175/JPO-D-15-0117.1

Cummings J A. 2005. Operational multivariate ocean data assimilation. Quarterly Journal of the Royal Meteorological Society, 131(613): 3583–3604, doi: 10.1256/qj.05.105

Du Yan, Qu Tangdong. 2010. Three inflow pathways of the Indonesian throughflow as seen from the simple ocean data assimilation. Dynamics of Atmospheres and Oceans, 50(2): 233–256, doi: 10.1016/j.dynatmoce.2010.04.001

Fang Guohong, Susanto D, Soesilo I, et al. 2005. A note on the South China Sea shallow interocean circulation. Advances in Atmospheric Sciences, 22(6): 946–954, doi: 10.1007/BF02918693

Fang Guohong, Susanto R D, Wirasantosa S, et al. 2010. Volume, heat, and freshwater transports from the South China Sea to Indonesian seas in the boreal winter of 2007–2008. Journal of Geophysical Research: Oceans, 115(C12): C12020, doi: 10.1029/2010JC006225

Fang Guohong, Wang Yonggang, Wei Zexun, et al. 2009. Interocean circulation and heat and freshwater budgets of the South China Sea based on a numerical model. Dynamics of Atmospheres and Oceans, 47(1–3): 55–72, doi: 10.1016/j.dynatmoce.2008.09.003

Fang Guohong, Wei Zexun, Choi B H, et al. 2003. Interbasin freshwater, heat and salt transport through the boundaries of the East and South China Seas from a variable-grid global ocean circulation model. Science in China Series D: Earth Sciences, 46(2): 149–161, doi: 10.1360/03yd9014

Fang Guohong, Wei Zexun, Huang Qizhou. 2002. Volume, heat and salt transports between the Southern South China Sea and its adjacent waters, and their contribution to the Indonesian Throughflow. Oceanologia et Limnologia Sinica (in Chinese), 33(3): 296–302

Gordon A L, Susanto R D, Vranes K. 2003. Cool Indonesian throughflow as a consequence of restricted surface layer flow. Nature, 425(6960): 824–828, doi: 10.1038/nature02038

He Zhigang, Feng Ming, Wang Dongxiao, et al. 2015. Contribution of the Karimata Strait transport to the Indonesian Throughflow as seen from a data assimilation model. Continental Shelf Research, 92: 16–22, doi: 10.1016/j.csr.2014.10.007

Lebedev K V, Yaremchuk M I. 2000. A diagnostic study of the Indonesian Throughflow. Journal of Geophysical Research: Oceans, 105(C5): 11243–11258, doi: 10.1029/2000JC900015

Liu Qinyan, Feng Ming, Wang Dongxiao. 2011. ENSO-induced interannual variability in the southeastern South China Sea. Journal of Oceanography, 67(1): 127–133, doi: 10.1007/s10872-011-0002-y

Liu Qinyan, Wang Dongxiao, Xie Qiang, et al. 2007. Decadal variability of Indonesian throughflow and South China Sea throughflow and its mechanism. Journal of Tropical Oceanography (in Chinese), 26(6): 1–6

Metzger E J, Hurlburt H E, Xu X, et al. 2010. Simulated and observed circulation in the Indonesian Seas: 1/12° global HYCOM and the INSTANT observations. Dynamics of Atmospheres and Oceans, 50(2): 275–300, doi: 10.1016/j.dynatmoce.2010.04.002

Qu Tangdong, Du Yan, Meyers G, et al. 2005. Connecting the tropical Pacific with Indian Ocean through South China Sea. Geophysical Research Letters, 32(24): L24609, doi: 10.1029/2005GL024698

Qu Tangdong, Du Yan, Sasaki H. 2006. South China Sea throughflow: a heat and freshwater conveyor. Geophysical Research Letters, 33(23): L23617, doi: 10.1029/2006GL028350

Qu Tangdong, Song Y T, Yamagata T. 2009. An introduction to the South China Sea throughflow: Its dynamics, variability, and application for climate. Dynamics of Atmospheres and Oceans, 47(1–3): 3–14

Schiller A, Godfrey J S, McIntosh P C, et al. 1998. Seasonal near-surface dynamics and thermodynamics of the Indian Ocean and Indonesian Throughflow in a global ocean general circulation model. Journal of Physical Oceanography, 28(11): 2288–2312, doi: 10.1175/1520-0485(1998)028<2288:SNSDAT>2.0.CO;2

Sprintall J, Wijffels S E, Molcard R, et al. 2009. Direct estimates of the Indonesian Throughflow entering the Indian Ocean: 2004–2006. Journal of Geophysical Research: Oceans, 114(C7): C07001

Sterlini P, De Vries H, Katsman C. 2016. Sea surface height variability in the North East Atlantic from satellite altimetry. Climate Dynamics, 47(3–4): 1285–1302, doi: 10.1007/s00382-015-2901-x

Su Jilan. 2005. Overview of the South China Sea circulation and its dynamics. Haiyang Xuebao (in Chinese), 27(6): 1–8

Susanto R D, Wei Zexun, Adi R T, et al. 2013. Observations of the Karimata Strait througflow from December 2007 to November 2008. Acta Oceanologica Sinica, 32(5): 1–6, doi: 10.1007/s13131-013-0307-3

Tozuka T, Qu Tangdong, Yamagata T. 2007. Dramatic impact of the South China Sea on the Indonesian throughflow. Geophysical Research Letters, 34(12): L12612, doi: 10.1029/2007GL030420

Tozuka T, Qu Tangdong, Masumoto Y, et al. 2009. Impacts of the South China Sea Throughflow on seasonal and interannual variations of the Indonesian Throughflow. Dynamics of Atmospheres and Oceans, 47(1–3): 73–85, doi: 10.1016/j.dynatmoce.2008.09.001

Wang Dongxiao, Liu Qinyan, Huang Ruixin, et al. 2006. Interannual variability of the South China Sea throughflow inferred from wind data and an ocean data assimilation product. Geophysical Research Letters, 33(14): L14605, doi: 10.1029/2006GL026316

Wei Jun, Li M T, Malanotte-Rizzoli P, et al. 2016. Opposite variability of Indonesian throughflow and South China Sea throughflow in the Sulawesi Sea. Journal of Physical Oceanography, 46(10): 3165–3180, doi: 10.1175/JPO-D-16-0132.1

Wu C R, Hsin Y C. 2012. The forcing mechanism leading to the Kuroshio intrusion into the South China Sea. Journal of Geophysical Research: Oceans, 117(C7): C07015

Wyrtki K. 1961. Physical oceanography of the southeast Asian waters. Scientific results of marine investigations of the South China Sea and the Gulf of Thailand 1959–1961. NAGA report, 2. California: University of California

Xie Qiang, Xiao Jin'gen, Wang Dongxiao, et al. 2013. Analysis of deep-layer and bottom circulations in the South China Sea based on eight quasi-global ocean model outputs. Chinese Science Bulletin, 58(32): 4000–4011, doi: 10.1007/s11434-013-5791-5

Yaremchuk M, McCreary Jr J, Yu Zuojun, et al. 2009. The South China Sea throughflow retrieved from climatological data. Journal of Physical Oceanography, 39(3): 753–767, doi: 10.1175/2008JPO3955.1

Zhang Zhengguang, Zhao Wei, Liu Qinyu. 2010. Sub-seasonal variability of Luzon Strait Transport in a high resolution global model. Acta Oceanologica Sinica, 29(3): 9–17, doi: 10.1007/s13131-010-0032-0